

First-principles study of magnetic structures of triangular antiferromagnets NaYbS₂ and NaYbO₂

Da-Ye Zheng, Zhen-Xiong Shen, Meng Zhang, and Lixin He*

CAS Key Laboratory of Quantum Information, University of Science and Technology of China, Hefei 230026, Anhui, China and Synergetic Innovation Center of Quantum Information and Quantum Physics,

University of Science and Technology of China, Hefei, 230026, China

(Dated: April 21, 2021)

We investigate the magnetic interactions in triangular rare-earth delafossites materials NaYbO₂ and NaYbS₂ via first-principles calculations. The calculated Curie-Weiss temperatures are in good agreement with experiments. We perform classical Monte Carlo simulations of the two compounds using the extracted exchange parameters. We find that if only the nearest neighbor interactions are considered, the magnetic ground states of NaYbO₂ and NaYbS₂ are a stripe and a planar 120° Néel state, respectively. The simulated transition temperatures are much higher than the lowest experimental temperatures, where no magnetic ordering was observed. However, we show by adding suitable second neighbor interactions, the *classical* magnetic ground state of NaYbO₂ becomes to the Z_2 vortex phase, and the simulated specific heat C_v are very similar to the experimental observations, with no obvious phase transition down to the extremely low temperature.

I. INTRODUCTION

Quantum spin liquids (QSL) are exotic states of matter, in which strong frustration and the quantum fluctuations prevent long-range magnetic ordering down to the zero temperature [1–4]. The QSL states are highly entangled, with novel excited state properties, such as emergent gauge fields and fractional particle excitations [3, 4], and therefore has attracted great attention since the concept had been proposed by Anderson [1].

One of the promising routines to search for the QSL is in the geometrically frustrated materials [5]. Recently, rare earth triangular lattice materials YbMgGaO₄ has been proposed to host a gapless QSL with effective-spin-1/2 local moments, in which no sign of long-range spin ordering has been observed down to the lowest temperature, $T \approx 50$ mK by various techniques [6–10]. However, it has been argued that the disordered spin state in YbMgGaO₄ might come from the Ga/Mg disorder, instead of true QSL [10–12]. On the other hand, the rare-earth delafossites AReCh₂ materials have perfect triangular layers, without the lattice distortion and site mixing in YbMgGaO₄. Very recently, high quality samples of a large family of AReCh₂ materials [13–15], including NaYbS₂ [16] and NaYbO₂ [17] have been synthesized. No magnetic ordering or transition in these materials are observed down to extremely low temperature from specific heat and susceptibility measurement. Therefore, they are ideal candidates for searching QSL.

It is well known that the ground state of the isotropic Heisenberg model on a triangular lattice is a planar 120° Néel state, instead of QSL [18]. Li et. al. proposed that the spin-orbit interactions may introduce anisotropic exchange interactions, which may add frustration to the model, leading to the QSL ground state [6, 7].

In this work, we investigate the magnetic properties of NaYbO₂ and NaYbS₂. We calculate the magnetic interactions in these materials, via first-principles calculations, and fit them to the anisotropic exchange model. The calculated Curie-Weiss temperatures are in good agreement with experiments. We then perform classical Monte Carlo simulations of the two materials, using the obtained exchange parameters, to investigate their finite temperature behaviors. We find that the ground state of NaYbS₂ is the planar 120° Néel state, whereas the ground state of NaYbO₂ has a stripe order, if only the nearest neighbor interactions are considered. The simulated transition temperatures are much higher than the lowest experimental temperatures, where no magnetic ordering was observed. However, we find that by adding suitable second nearest neighboring exchange interactions, the magnetic ground state becomes the Z_2 vortex. The simulated specific heat C_v are very similar to the experimental observations, with no obvious phase transition down to the extremely low temperature.

II. METHODS

The electronic and magnetic properties are calculated via density functional theory, within the generalized gradient approximation of the Perdew-Burke-Ernzerhof (PBE) [19], implemented in Vienna ab initio simulations package (VASP) [20]. The projector-augmented wave (PAW) pseudopotentials with spin-orbit couplings (SOC) are used. A 500 eV plane-wave energy cutoff results in very fast convergence. The on-site Coulomb interactions $U-J=6.0$ eV are included for Yb 4*f* electrons in a rotationally invariant scheme [21]. The experimental crystal structures are used for the calculation [22, 23]. For calculations using primitive unit cells, an $11 \times 11 \times 11$ k -point mesh is used, whereas a $9 \times 9 \times 4$ k -point mesh is used for the calculations on the conventional unit cell, containing 48 atoms.

* helx@ustc.edu.cn

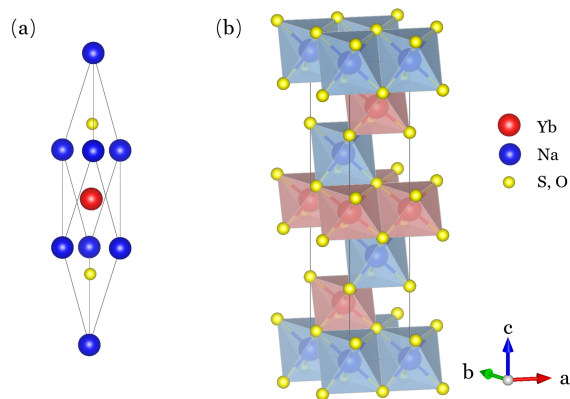


FIG. 1. (Color online) (a) The primitive unit cell and (b) a $\sqrt{3}\times\sqrt{3}\times 1$ conventional unit cell of NaYbS_2 . The Yb^{3+} ions are located in the center of YbS_6 octahedrons, which have an ABAB stacking along the c axis, separated by the Na layers.

III. RESULTS AND DISCUSSION

A. Crystal structures

The NaReCh_2 (where $\text{Ch}=\text{O}, \text{S}$ and $\text{Re}=\text{Yb}, \text{Ga}, \text{Tb}$ are the rare-earth ions) is a large family of materials, which have an ideal triangular lattice structure, with space group $R\bar{3}m$. In this work, we focus on the properties of two representative compounds: NaYbS_2 , and NaYbO_2 .

Figure 1(a) depicts the structure of the primitive unit cell of NaYbS_2 , containing four atoms, whereas a $\sqrt{3}\times\sqrt{3}\times 1$ conventional unit cell is shown in Fig. 1(b). The Yb^{3+} ion and its six surrounding S ions form a YbS_6 octahedron. The Yb^{3+} ions are located at the centers of the octahedrons, which are the centers of the D_{3d} symmetry [17], precluding any Dzyaloshinskii–Moriya [24, 25] distortions. Indeed, the Na NMR lines reveal an absence of inherent structural distortions in NaYbS_2 [26], and NaYbO_2 [17]. Therefore, the Yb^{3+} ions form a perfect triangular quasi-2D lattice. This is in strong contrast to the well-explored spin-liquid candidate YbMgGaO_4 [6–10], which has considerable site mixing of the Ga and Mg ions. The YbS_6 octahedrons have an ABAB stacking along the c axis, separated by the Na layers, and the magnetic coupling between different Yb^{3+} layers are expected to be negligible. The lattice constants of NaYbS_2 are $a=3.901 \text{ \AA}$ and $c=19.736 \text{ \AA}$ [22], which are much larger than those of NaYbO_2 , $a=3.346 \text{ \AA}$ and $c=16.456 \text{ \AA}$ [23].

B. Band structures

Figure 2(a),(c) depict the electrical bands structures of NaYbS_2 and NaYbO_2 respectively, and the corresponding partial density of states (PDOS) for Na $3s$, Yb $4f$ and S/O p electrons are shown in Fig. 2(b),(d). The PDOS of Na $3s$ electrons are marginal in this energy window

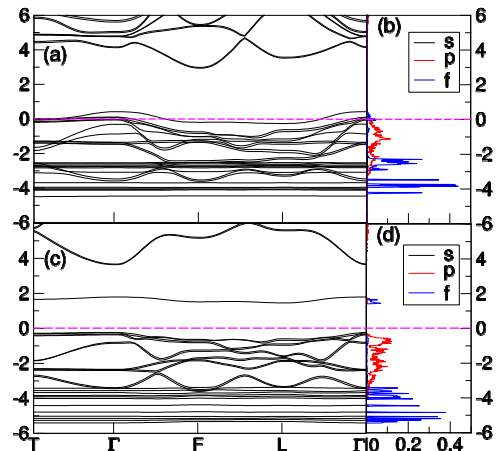


FIG. 2. (Color online) Left: The band structures of (a) NaYbS_2 and (c) NaYbO_2 . Right: The corresponding PDOS of Na $3s$, S $3p$ (O $2p$), and Yb $4f$ orbitals are shown in (b) and (d) respectively. The dashed line denotes the Fermi level.

as shown in the figures. The band structures and PDOS are calculated using primitive unit cells with the FM spin configuration, i.e., all spin of Yb^{3+} ions are forced to align along the z -axis, with SOC turned on. The Fermi levels are dominated by the S/O p orbitals. The Yb $4f$ electrons form rather flat bands, which are about 2 - 4 eV below the Fermi level for NaYbS_2 , and about 4 - 6 eV below the Fermi level for NaYbO_2 . These results suggest that the Yb $4f$ states are very localized, with only small hybridization between the Yb $4f$ and S/O p electrons. But still, one can see that the Yb $4f$ electrons hybridize stronger with the S p orbitals than with the O p orbitals.

Experimentally, NaYbS_2 and NaYbO_2 are insulators, with band gaps equal 2.7 eV and 4.5 eV respectively [13]. However, there are about 0.83 electrons per unit cell above the Fermi level for NaYbS_2 calculated by the DFT+U method. The NaYbO_2 turns out to be an insulator from the DFT+U calculations, however, the calculated bandgap is 1.70 eV, which is also significantly smaller than the experimental values. These results suggest that NaYbS_2 and NaYbO_2 are strongly correlated materials, and may not be well described by the DFT+U method, which treats the on-site Coulomb U in an oversimplified mean-field way. To accurately calculate the electronic structure of NaYbS_2 , and NaYbO_2 is an interesting and challenging problem, which may require more sophisticated many-particle techniques (e.g. dynamics mean-field theory[27]) to treat the strong correlation effects. Despite this, we would still like to calculate the magnetic interactions in these materials to shed some light on possible QSL states in these materials.

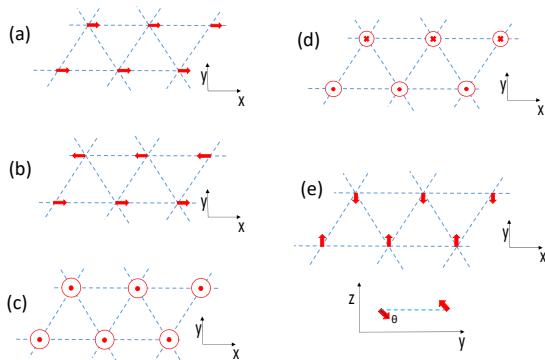


FIG. 3. (Color online) The spin configurations used to fit the exchange parameters: (a) All spins are parallel along the x axis (FM $_x$); (b) The spins have a stripe order along the x axis (x -stripe); (c) All spins are parallel along the z axis (FM $_z$); (d) The spins have a stripe order along the z axis (z -stripe); (e) The spins have a stripe order in the yz plane, with $\theta = \pi/4$ (yz -stripe).

C. Magnetic exchange interactions

In NaYbS₂ and NaYbO₂, the $4f$ electrons of Yb³⁺ ions couple strongly to the orbital momentum, resulting in a total angular momentum $J=7/2$ state, which splits under the crystal field. It has been shown that the ground state spin doublet is well separated from the excited spin doublets [7], and therefore, the system can be treated as an effectively spin-1/2 system. The strong SOC coupling in these materials further introduces anisotropic magnetic exchange interactions [6, 7, 28]. We would first like to extract the magnetic exchange interactions as input parameters for further studies.

Li et al. derived a general Heisenberg model Hamiltonian based on symmetry consideration for the triangular compounds [7]. The Hamiltonian reads, following the notation of Ref.29,

$$\begin{aligned} \mathcal{H} = \sum_{\langle ij \rangle} \{ & J (S_i^x S_j^x + S_i^y S_j^y + \Delta S_i^z S_j^z) \\ & + 2J_{\pm\pm} [(S_i^x S_j^x - S_i^y S_j^y) \tilde{c}_\alpha - (S_i^x S_j^y + S_i^y S_j^x) \tilde{s}_\alpha] \\ & + J_{z\pm} [(S_i^y S_j^z + S_i^z S_j^y) \tilde{c}_\alpha - (S_i^x S_j^z + S_i^z S_j^x) \tilde{s}_\alpha] \} \end{aligned} \quad (1)$$

where $\tilde{c}(\tilde{s})_\alpha = \cos(\sin)\tilde{\phi}_\alpha$, and $\tilde{\phi}_\alpha = \{0, 2\pi/3, -2\pi/3\}$ are the bond angles with respect to the x -axis. The first term of Eq.(1) is the standard XXZ model and is invariant under the global spin rotation around the z -axis. The $J_{\pm\pm}$ and $J_{z\pm}$ terms define the bond dependent anisotropic interactions caused by the strong SOC, and sometimes are called the pseudo-dipolar terms [30].

To obtain the J , Δ , $J_{\pm\pm}$ and $J_{z\pm}$ parameters, we fit the model to the total energies of five spin configurations, including FM $_x$, FM $_z$, x -stripe, z -stripe, yz -stripe states, which are schematically shown in Fig. 3. The per-site

energies [in units of $S(S+1)$] of these chosen classical spin configurations are as follows:

$$\begin{aligned} E_{\text{FM}_x} &= 3J, \\ E_{\text{FM}_z} &= 3J\Delta, \\ E_{x\text{-stripe}} &= -J + 4J_{\pm\pm}, \\ E_{z\text{-stripe}} &= -J\Delta, \\ E_{yz\text{-stripe}} &= -\tilde{J}_c - \Delta J - \sqrt{4J_{z\pm}^2 + \tilde{J}_c^2}, \end{aligned} \quad (2)$$

where $\tilde{J}_c = [J(1 - \Delta) + 4J_{\pm\pm}]/2$.

To accommodate the above magnetic states, we adopt a supercell containing the $2 \times 2 \times 1$ conventional unit cell of Fig. 1(b). A $9 \times 9 \times 4$ k -point mesh is used to ensure the convergence of the total energies.

TABLE I. The total energies (in eV) of the five spin configurations shown in Fig.3.

	FM $_z$	FM $_x$	z -stripe	x -stripe	yz -stripe
NaYbS ₂	-201.123	-201.121	-201.234	-201.233	-201.233
NaYbO ₂	-264.303	-264.302	-264.317	-264.315	-264.316

TABLE II. The exchange parameters fitted from total energies of different spin configurations.

	J (K)	Δ	$J_{\pm\pm}/J$	$J_{z\pm}/J$	θ_{CWx}	θ_{CWz}	θ_{CW}^{exp}
NaYbS ₂	36.660	0.980	1.80%	2.96%	-54.99	-53.87	-63.74[13] -65 [26]
NaYbO ₂	5.039	0.889	12.81%	21.1%	-7.56	-6.72	-6 [15] -5.64[31]

The calculated total energies of NaYbS₂ and NaYbO₂ with the five spin configurations are listed in Table I, and the fitted exchange parameters are listed in Table II. The Curie-Weiss (CW) temperatures θ_{CW} are estimated as $\theta_{CWx} = -\frac{3}{2}J$, whereas $\theta_{CWz} = -\frac{3}{2}\Delta J$ [6, 31]. Experimentally, θ_{CW} is fitted from the magnetic susceptibility $1/\chi(T)$ via the Curie-Weiss law. We mark that θ_{CW} depend strongly on the fitting temperature. For example, Curie-Weiss temperature is $\theta_{CW} = -65$ K for NaYbS₂ when fitting $1/\chi(T)$ below 80K [26]. However, $\theta_{\perp} = -13.5$ K which fitted below 10 K and $\theta_{\parallel} = -4.5$ K which fitted below 5 K [26]. Here, \perp and \parallel refer to that a small magnetic field is applied perpendicular or parallel to the c axis, respectively, when measuring $\chi(T)$. We compare the calculated θ_{CW} to the experimental results fitted at higher temperatures. This is because, at low temperature, the magnetic state tends to be in a strongly correlated (highly entangled) state, whereas at a higher temperature, the spins are more like the classical spin states, which are more appropriate for the mean-field description.

The calculated θ_{CW} of NaYbS₂ is about 54 K, and that of NaYbO₂ is about 6 K, both are in very good agreement with experimental results [13, 15, 17, 26, 31].

At first glance, it is somehow surprising, that the magnetic exchange interactions in NaYbS_2 are even stronger than those of NaYbO_2 , given that the lattice constants of NaYbS_2 ($a=3.901\text{\AA}$) are larger than those of NaYbO_2 ($a=3.346\text{\AA}$), due to the larger ion radii of S ions. However, as seen from the PDOS shown in Fig. 2(b) and Fig. 2(d), the Yb $4f$ electrons hybridize more strongly with S $3p$ electrons than with O $2p$ electrons, which leads to larger super-exchange interactions.

The SOC interactions introduce the anisotropic magnetic interactions. From Table II, we see that the anisotropy is rather small in NaYbS_2 , as $\Delta \approx 0.98$ (where $\Delta=1$ is the isotropic case). The anisotropic exchanges $J_{\pm\pm}/J \approx 0.018$ and $J_{z\pm}/J \approx 0.03$ are also quite small. NaYbO_2 shows somehow stronger anisotropy, with $\Delta \approx 0.89$, $J_{\pm\pm}/J \approx 0.128$ and $J_{z\pm}/J \approx 0.211$.

D. Magnetic phase diagram of classical spin model

The phase diagrams of the classical spin model in Eq. 1 has been studied via spin-wave [29] and classical Monte Carlo method [7, 12, 32, 33]. In the vicinity of isotropic region, i.e., $\Delta \approx 1$, $J_{\pm\pm}/J \approx 0$ and $J_{z\pm}/J \approx 0$, the ground state of model Eq. 1 is a planar 120° Néel state. For $J_{\pm\pm}/J \lesssim -0.15$, the system has a stripe- x order, in which the spins lie within the x - y plane [29], whereas for $J_{\pm\pm}/J \gtrsim -0.15$, the system is in the stripe- yz order, where spins are partially out of the x - y plane [29]. Between the stripe phases and the planar 120° phase, there are also so-called multi- Q phase, where the spins are incommensurate and ordered at multiple Q vectors [32]. In the Heisenberg limit, spin-wave results suggest that the multi- Q state is similar to the Z_2 vortex state which has been found in the triangular Kitaev-Heisenberg model [34, 35].

The quantum spin model has been studied using DMRG methods [36], and the results suggest that there exists a QSL phase instead of multi- Q phase within the region $J_{z\pm} \simeq [0.27, 0.45]$ and $J_{\pm\pm} \simeq [-0.17, 0.1]$ in the isotropic limit $\Delta=1$. The exact diagonalizations [37] of small clusters of 12 - 32 sites also suggest that there is a spin liquid region, but the spin structure factors are different from the DMRG results. However, very recently projected entangled pair states (PEPS) [38–40] calculations show that there is no QSL in the phase-diagram [33]. The nature of the quantum phase in this region is still under debate.

Nevertheless, the calculated exchange interaction parameters for NaYbS_2 and NaYbO_2 are far away from the DMRG calculated QSL region. In fact, the parameters calculated for NaYbS_2 is very close to the isotropic region, and the ground state is the planar 120° Néel state, whereas the ground state of NaYbO_2 is of the stripe- yz order.

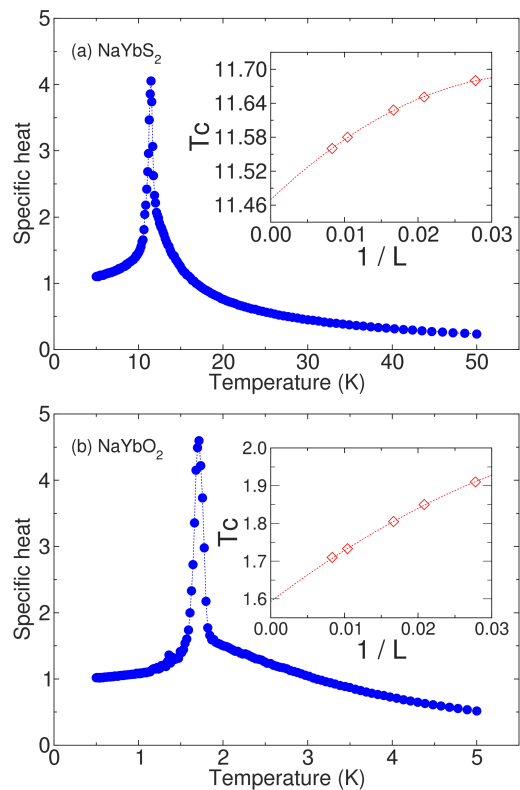


FIG. 4. (Color online) The simulated specific heat (blue dots) as functions of temperature for (a) NaYbS_2 and (b) NaYbO_2 by using Hamiltonian Eq. 1. The simulations are performed on a 120×120 lattice. The inserts depict the transition temperatures T_c as functions of $1/L$.

1. Nearest Neighbor Model

To investigate the magnetic phase transitions of NaYbO_2 , and NaYbS_2 , we perform replica-exchange Monte Carlo (MC) simulations [41] of the classical spin model of Eq. 1, using the exchange parameters obtained from first-principles calculations Sec.III C. The simulations are performed on the $L \times L$ lattices, where $L=36, 48, 60, 96$, and 120 .

Figure 4(a),(b) depict the specific heats as functions of temperature for NaYbS_2 and NaYbO_2 respectively on a 120×120 lattice. For NaYbO_2 , the specific heat shows a sharp peak near the temperature of 1.7 K. In the insert of the figure, we plot the transition temperature calculated on different lattice sizes. By finite-size scaling, the transition temperature in the thermodynamic limit is about 1.6 K. The magnetic transition for NaYbS_2 is about 11.6 K for 120×120 lattice and about 11.5 K in the thermodynamic limit as shown in Fig. 4(b). These transition temperatures are much too high compared to the experimental results, where no magnetic transition was observed down to 50 mK for NaYbO_2 [17] and 260 mK for NaYbS_2 [26].

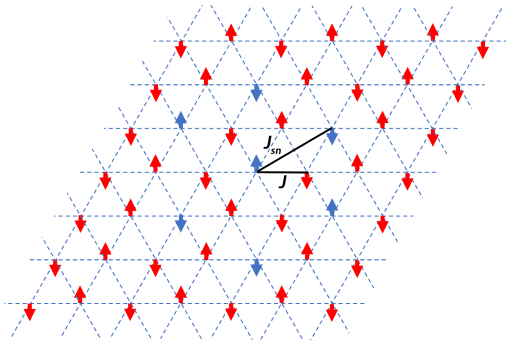


FIG. 5. (Color online) The ground state spin configuration of NaYbO₂ with only the NN interactions is of a yz -stripe order. A spin and all its NNN spins are shown in blue. J and J_{sn} are the NN and NNN exchange interactions respectively.

2. Second Neighbor Model

Given the above MC simulation results, we conclude that the experimentally observed magnetic disorder states of NaYbO₂ and NaYbS₂ are unlikely to be described by the nearest-neighbor (NN) interaction models. To understand the experimental results, we try to include the next nearest neighboring (NNN) interactions in the MC simulations. We consider the simplest NNN interactions, which take the form of,

$$\mathcal{H}_{\text{NNN}} = \sum_{\langle\langle i,j \rangle\rangle} J_{sn}(S_i^x S_j^x + S_i^y S_j^y + \Delta S_i^z S_j^z) \quad (3)$$

Since the first-principles calculations of the NNN exchanges, which require very large supercells, are extremely difficult for the geometrically frustrated materials NaYbO₂ and NaYbS₂, we take the NNN exchange interaction J_{sn} as a parameter, which varies in the range of $-0.2J$ to $0.2J$.

Here, we focus on the results of NaYbO₂ in the following discussions. The ground state spin configuration for NaYbO₂ with NN exchange interactions is shown in Fig. 5, which is in a yz -stripe order. A spin and all its NNN spins are shown in blue. The transition temperature as a function of NNN exchange interaction J_{sn} is shown in Fig. 6. The simulations are carried out on a 48×48 lattice. At $J_{sn}=0$, the magnetic ground state is in a yz -stripe order. When increasing J_{sn} from 0 to $0.2J$, the magnetic ground state does not change, whereas the transition temperature gradually increases with the increasing of J_{sn} , and reaches about 3 K at $J_{sn}=0.2J$. To understand the results, we note that for each spin on the lattice, there are six NNN spins around it, as shown in Fig. 5. In the yz -stripe phase, two-third of NNN spins are antiparallel to the central spin and the other one-third of spins are parallel to it. When a positive J_{sn} in Eq. 3 is used, the NNN interactions further stabilize the magnetic order and therefore increase the transition temperature.

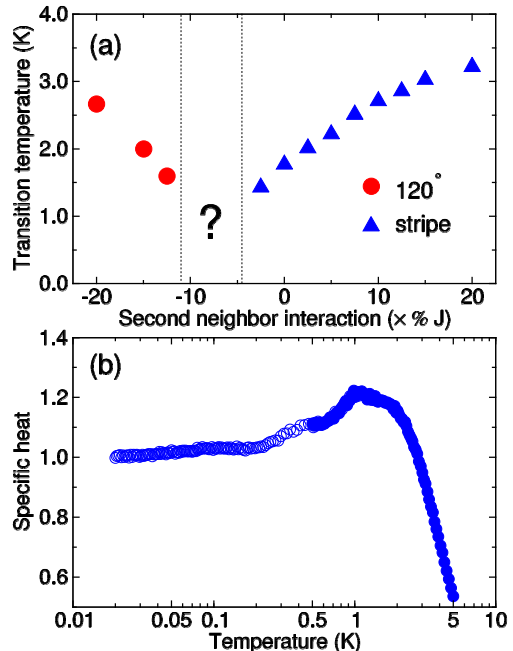


FIG. 6. (Color online) (a) The transition temperature T_c as a function of J_{sn} . For $J_{sn} \leq -0.125J$, the ground state is the planar 120° Néel state (red circles), whereas for $J_{sn} > -0.05J$, the ground state is of yz -stripe order (blue triangles). For $-0.1J \leq J_{sn} \leq -0.05J$, the ground state is a Z_2 vortex phase, with no sharp phase transitions. (b) The specific heat as function of temperature for $J_{sn} = -0.05J$.

When a negative J_{sn} is added, the NNN interactions add more frustration to the yz -stripe order which will decrease the Curie temperature as shown in Fig. 6. For $J_{sn} \leq -0.125J$, the ground state becomes to the planar 120° Néel state, and the transition temperature raises with the decreasing J_{sn} .

Remarkably, for $-0.1J \leq J_{sn} \leq -0.05J$, we find no obvious phase transition down to the lowest simulation temperature of 20 mK. The specific heat as a function of temperature for $J_{sn} = -0.05J$ has a very broad peak as shown in Fig. 6(b), which is very similar to the C_v curve for NaYbO₂ at $H=0$ [17]. In the experiments, C_v approach zero as temperature approaching zero [17], while C_v approach a finite value in our simulation. This might be because we use a classical model, instead of a quantum model. The ground state spin configuration is shown in Fig. 7, which can be identified as a Z_2 vortex phase [33–35]. The broad C_v curve is due to the Kosterlitz-Thouless (KT) melting of the Z_2 vortex [42]. We note that recently the KT transition has also been proposed by Li et. al. for TmMgGaO₄ [43]. Whether the Z_2 ground state will melt at zero temperature due to quantum fluctuation resulting in a QSL state, requires further studies.

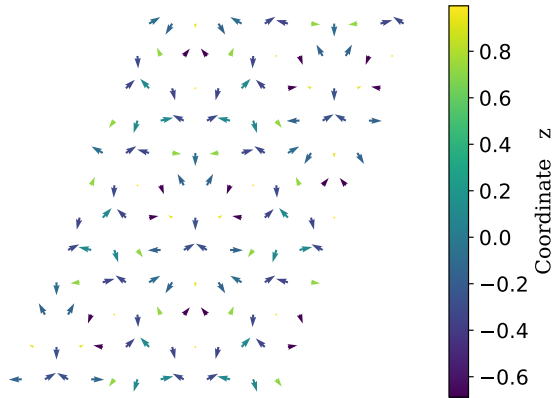


FIG. 7. (Color online) The ground state spin configure of the Z_2 vortex phase. The arrows show the x, y components of the spins, whereas the color marks the z component.

IV. SUMMARY

We calculate the magnetic interactions in NaYbO_2 and NaYbS_2 via the first-principles method. The calculated Curie-Weiss temperatures are in good agreement with

experiments. We then perform classical MC simulations of the finite-temperature phase diagram of the two compounds using the extracted phase exchange parameters. We find that if only the nearest neighbor interactions are considered, the ground states are a stripe and a planar 120° Néel state for NaYbO_2 and NaYbS_2 , respectively. The simulated transition temperatures are much higher than the lowest experimental temperatures, where no magnetic ordering was observed. These results suggest that the experimentally observed magnetic disorder states of NaYbO_2 and NaYbS_2 are unlikely to be described by the nearest-neighbor interaction models. We show by adding suitable second neighboring interactions, the classical magnetic ground state of NaYbO_2 becomes to the Z_2 vortex phase, and the simulated specific heat C_v has a very broad peak, which is due to the KT melting of the Z_2 vortex. Whether the Z_2 ground state will melt due to quantum fluctuation at zero temperature resulting in a QSL state is an interesting topic for future studies.

ACKNOWLEDGMENTS

This work is funded by the Chinese National Science Foundation Grant number 11774327. The numerical calculations were done on the USTC HPC facilities.

-
- [1] P. W. Anderson, *Mater. Res. Bull.* **8**, 153 (1973).
 - [2] P. W. Anderson, *Science* **235**, 1196 (1987).
 - [3] L. Balents, *Nature* **464**, 199 (2010).
 - [4] L. Savary and L. Balents, *Rep. Prog. Phys.* **80**, 016502 (2017).
 - [5] C. Lacroix, P. Mendels, and F. Mila, eds., *Introduction to Frustrated Magnetism* (Springer-Verlag, Berlin Heidelberg, 1988).
 - [6] Y. Li, G. Chen, W. Tong, L. Pi, J. Liu, Z. Yang, X. Wang, and Q. Zhang, *Phys. Rev. Lett.* **115**, 167203 (2015).
 - [7] Y.-D. Li, X. Wang, and G. Chen, *Phys. Rev. B* **94**, 035107 (2016).
 - [8] Y. Li, D. Adroja, P. K. Biswas, P. J. Baker, Q. Zhang, J. Liu, A. A. Tsirlin, P. Gegenwart, and Q. Zhang, *Phys. Rev. Lett.* **117**, 097201 (2016).
 - [9] Y. Shen, Y.-D. Li, H. Wo, Y. Li, S. Shen, B. Pan, Q. Wang, H. C. Walker, P. Steffens, M. Boehm, et al., *Nature* **540**, 559 (2016).
 - [10] J. A. M. Paddison, M. Daum, Z. Dun, G. Ehlers, Y. Liu, M. Stone, H. Zhou, and M. Mourigal, *Nat. Phys.* **13**, 117 (2017).
 - [11] Z. Zhu, P. A. Maksimov, S. R. White, and A. L. Chernyshev, *Phys. Rev. Lett.* **119**, 157201 (2017).
 - [12] E. Parker and L. Balents, *Phys. Rev. B* **97**, 184413 (2018).
 - [13] W. Liu, Z. Zhang, J. Ji, Y. Liu, J. Li, X. Wang, H. Lei, G. Chen, and Q. Zhang, *Chinese Phys. Lett.* **35**, 117501 (2018).
 - [14] J. Xing, L. D. Sanjewa, J. Kim, G. R. Stewart, A. Podlesnyak, and A. S. Sefat, *Phys. Rev. B* **100**, 220407(R) (2019).
 - [15] K. M. Ranjith, S. Luther, T. Reimann, B. Schmidt, P. Schlender, J. Sichelschmidt, H. Yasuoka, A. M. Strydom, Y. Skourski, J. Wosnitza, et al., *Phys. Rev. B* **100**, 224417 (2019).
 - [16] R. Sarkar, P. Schlender, V. Grinenko, E. Haeussler, P. J. Baker, T. Doert, and H.-H. Klauss, *Phys. Rev. B* **100**, 241116(R) (2019).
 - [17] M. M. Bordelon, E. Kenney, C. Liu, T. Hogan, L. Posthuma, M. Kavand, Y. Lyu, M. S. Sherwin, N. P. Butch, C. M. Brown, et al., *Nat. Phys.* **15**, 1058 (2019).
 - [18] L. Capriotti, A. E. Trumper, and S. Sorella, *Phys. Rev. Lett.* **82**, 3899 (1999).
 - [19] J. P. Perdew, K. Burke, and M. Ernzerhof, *Phys. Rev. Lett.* **77**, 3865 (1996).
 - [20] G. Kresse and J. Furthmüller, *Phys. Rev. B* **54**, 11169 (1996).
 - [21] S. L. Dudarev, G. A. Botton, S. Y. Savrasov, C. J. Humphreys, and A. P. Sutton, *Phys. Rev. B* **57**, 1505 (1998).
 - [22] T. Schleid and F. Lissner, *European journal of solid state and inorganic chemistry* **30**, 829 (1993).
 - [23] Y. Hashimoto, M. Wakeshima, and Y. Hinatsu, *Journal of Solid State Chemistry* **176**, 266 (2003).
 - [24] I. E. Dzyaloshinskii, *Sov. Phys. JETP* **19**, 960 (1964).
 - [25] T. Moriya, *Phys. Rev.* **120**, 91 (1960).

- [26] M. Baenitz, P. Schlender, J. Sichelschmidt, Y. A. Onykiienko, Z. Zangeneh, K. M. Ranjith, R. Sarkar, L. Hozoi, H. C. Walker, J.-C. Orain, et al., *Phys. Rev. B* **98**, 220409(R) (2018).
- [27] A. Georges, G. Kotliar, W. Krauth, and M. J. Rozenberg, *Rev. Mod. Phys.* **68**, 13 (1996).
- [28] W. Witczak-Krempa, G. Chen, Y. B. Kim, and L. Balents, *Annual Review of Condensed Matter Physics* **5**, 57 (2014).
- [29] P. A. Maksimov, Z. Zhu, S. R. White, and A. L. Chernyshev, *Phys. Rev. X* **9**, 021017 (2019).
- [30] J. Iaconis, C. Liu, G. B. Halasz, and L. Balents, *SciPost Phys.* **4**, 3 (2018).
- [31] L. Ding, P. Manuel, S. Bachus, F. Gruffer, P. Gegenwart, J. Singleton, R. D. Johnson, H. C. Walker, D. T. Adroja, A. D. Hillier, et al., *Phys. Rev. B* **100**, 144432 (2019).
- [32] C. Liu, R. Yu, and X. Wang, *Phys. Rev. B* **94**, 174424 (2016).
- [33] Zheng, Meng and Chao Wang and Yongjian Han and Lixin He, unpublished.
- [34] I. Rousochatzakis, U. K. Rössler, J. van den Brink, and M. Daghofer, *Phys. Rev. B* **93**, 104417 (2016).
- [35] M. Becker, M. Hermanns, B. Bauer, M. Garst, and S. Trebst, *Phys. Rev. B* **91**, 155135 (2015).
- [36] Z. Zhu, P. A. Maksimov, S. R. White, and A. L. Chernyshev, *Phys. Rev. Lett.* **120**, 207203 (2018).
- [37] M. Wu, D.-X. Yao, and H.-Q. Wu, arXiv:2008.08751 [cond-mat] (2020).
- [38] F. Verstraete and J. I. Cirac, cond-mat/0407066 (2004).
- [39] F. Verstraete, V. Murg, and J. Cirac, *Advances in Physics* **57**, 143 (2008).
- [40] W.-Y. Liu, S. Dong, C. Wang, Y. Han, H. An, G.-C. Guo, and L. He, *Phys. Rev. B* **98**, 241109(R) (2018).
- [41] K. Cao, G.-C. Guo, D. Vanderbilt, and L. He, *Phys. Rev. Lett.* **103**, 257201 (2009).
- [42] H. Kawamura and S. Miyashita, *J. Phys. Soc. Jpn.* **53**, 4138 (1984).
- [43] H. Li, Y. D. Liao, B.-B. Chen, X.-T. Zeng, X.-L. Sheng, Y. Qi, Z. Y. Meng, and W. Li, *Nat. Commun.* **11**, 1111 (2020).